The ball on three balls test for strength testing of brittle discs: stress distribution in the disc

Andreas Börger*, Peter Supancic, Robert Danzer

Department for Structural and Functional Ceramics, University of Leoben, A-8700 Leoben, Austria

Abstract

Biaxial strength testing of brittle materials is claimed to have some benefits compared to uniaxial testing, e.g. the much simpler specimen preparation, the avoiding of tensile loaded edges, the similarity of the stress state to those from typical loading (e.g. during a thermal shock loading) and the fact, that biaxial stress states are more revealing of defects than uniaxial stress states. The experience of the past showed, that biaxial strength testing has its own problems, to avoid these led to the development of several variants. One of these variants, the ball on three balls test, seems to be extremely simple: a disc is supported by three balls and then axially loaded from the opposite side via a fourth ball. In this system small deviations from the requested geometry, especially some out of flatness of the disc, are mentioned to be tolerable, but the threefold bending symmetry makes an exact analytical assessment of the stress state in the loaded disc extremely difficult. A numerical approach has yet not been performed. In this paper a FE analysis of the stress state in a ball on three balls tested disc is performed. The stress field scales with the maximum principle stress, which occurs in the centre of the tensile surface. For this stress an analytical approximation (which has been fitted to the numerical results) is given, which accounts for the influence of all relevant geometrical and material parameters. The investigated range of parameters considers the values typical for testing of brittle materials. © 2002 Elsevier Science Ltd. All rights reserved.

Keywords: Ball on three balls test, Finite element analysis, Mechanical properties, Strength, Testing

1. Introduction

Biaxial strength testing of brittle materials has been used for many years, and there exists a wide variety of test assemblies described in the literature. Typically, there are several advantages claimed for biaxial flexural testing of discs compared with uni-axial testing (in tension or in bending), including ease of test piece preparation, use for thin sheet materials and testing of a large surface area free from edge finishing defects.[1] Furthermore the biaxial stress distribution is more searching for defects than a uni-axial distribution.[2] Many commercially produced components are biaxially loaded and for them biaxial testing is the more relevant test condition.

The most common biaxial test assemblies are listed in Table 1, which are generally applied for "thin" discs. Often used is an axisymmetrical testing assembly where the disc is supported by a ring and loaded from the opposite side by another, smaller concentric ring (ring-on-

ring test).[3,4] In the area underneath the smaller ring exists an equi biaxial tensile stress state where initialisation of fracture is expected. Alternatively the ball-on-ring test[5] and the ball on ring of balls test[6] are also often used. All three methods show the disadvantage, that more or less perfect flat discs are required,[2] which might make polishing of the specimens necessary. Any deviations from flatness lead to additional stresses during the loading, so that strength results become hardly interpretable. Therefore, the punch on three balls test has been developed, which tolerates a small out of flatness of the disc,[3] since also non planar discs faces are supported stably by three points. It is standardised in ATSM F 394-78.[7] In that standard and the related literature[3] only small variations of the geometry are considered which strictly limits the applicability of this test assembly. Variants of these tests are the ring of balls on ring of balls test, the full or part pressurisation of ring supported disc test,[5] the punch on ring test,[5] the ball with flat on ring test[5] and the ball with a flat on three balls tests.[9]

Another familiar test geometry and topic of this article, the ball on three balls test,[6] is even more tolerant to

---

* Corresponding author.
  E-mail address: isfk@unileoben.ac.at (A. Börger).

Table 1
Typical testing assemblies for bi-axial strength test of discs with (a) axis-symmetric and (b) non axis-symmetric stress distributions

	Reference
(a) Axis-symmetric stress distribution	
Ring on ring	ISO 6474,[13] Soltesz et al.,[3]Fessler and Fricker[4]
Ball on ring	Matthewson and Field[5]
Punch on ring	Matthewson and Field[5]
Ball with flat on ring	Matthewson and Field[5]
Full or part pressurisation of ring supported disc	Matthewson and Field[5]
(b) Non axis-symmetric stress distribution	
Punch on three balls	ASTM F394,[7] Kirstein and Woolley[8]
Ball on three balls	Godfrey[10]
Ball on ring of balls	Godfrey and John[6]
Ring of balls on ring of balls	Godfrey and John[6]
Ball with flat on three balls	Byrne and Morrell[9]

some out of flatness of the disc then all other test assemblies mentioned above. In general sintered discs with no special surface finishing can be tested, allowing a quick testing of samples, e.g. during production for quality control. In this test the lower face of a disc specimen is supported on three balls equidistant from its centre. The upper face is centrally loaded with a fourth ball. The fracture load is measured. The strength is defined to be the maximum principal tensile stress in the disc, which occurs on the disc surface opposite the centred loading ball. Of course the stress field in the disc depends on the applied load, on the geometric set-up of the test, namely the thickness and the diameter of the disc and the size and the position of the balls, and also on the elastic properties of ball and disc materials. The proper evaluation of the ball on three balls test needs the exact knowledge of this relationship between applied load and the maximum tensile stress but up to now, a systematic study is still missing.

Some analytical approximations for the stress distribution in the disc exists[8,10–12] which all are insufficient for two main reasons. Firstly all of them are based on the cylindrical symmetrical thin-plate-theory that predicts an infinite tensile stress amplitude (i.e. a logarithmic singularity) opposite to the load transfer point, modelled as a point force. Therefore, the approximations fail to describe the tensile stresses opposite the loading area in the centre of the disc. Secondly the approximations depend on the contact radius between the loading ball and the disc and as will be shown later, none of the given solutions is appropriate. Table 2 shows several of these approximations, which predict very different contact radii leading to different results for the tensile stress distribution around the centre of the disc.

In this paper a finite element analysis of the stress fields in ball on three ball-loaded discs is performed. An analytic expression for the relation between load and maximum stress in dependence of the testing geometry for the practical evaluation of this tests will be derived. First testing results on a commercial Al_2O_3 ceramic are presented.

Table 2
Approximations for the contact radius b of the central loading ball

	b	
Westergaard[14]	t	for $\zeta > 1.724t$
	$(1.6\zeta^2 + t^2)^{1/2} - 0.675t$	for $0 \leqslant \zeta \leqslant 1.724t$
Godfrey[10]	$0.721 \cdot \left[F \cdot 2R_b \cdot \dfrac{1}{E'} \right]^{\frac{1}{3}}$	for $\zeta \geqslant 0$
Shetty et al.[15]	$t/3$	for $\zeta \geqslant 0$

2. Analytical solutions for the ball on three balls test

Different approaches have been made for the analytical calculation of the stress distribution in centrally loaded biaxial disc tests. They are all based on the linear-elastic axisymmetric thin-plate theory. Basic work was done by Bassali[11] and later in a more specified way by Kirstein and Woolley.[8] According to Kirstein and Woolley the maximum tensile stress σ_{max} in the centre of the disc face is approximately independent from the number of support points and can be described by:

$$\sigma_{max} = -\frac{3 \cdot F}{4 \cdot \pi \cdot t^2} (\xi - \lambda), \tag{1}$$

where

$$\xi = (1 + \nu) \cdot \ln\left(\frac{b}{R}\right)^2 + \frac{(1 - \nu)}{2} \cdot \left(\frac{b}{R}\right)^2, \tag{2}$$

and

$$\lambda = (1 + \nu) \cdot \left[1 + \ln\left(\frac{R_a}{R}\right)^2 \right] + (1 - \nu) \cdot \left(\frac{R_a}{R}\right)^2, \tag{3}$$

with F, applied load;
 t, sample thickness;
 ν, Poisson's ratio of the disc material;

b, radius of the loaded area (e.g. contact radius of the loading ball or loading pinch on the disc, assumed to be under constant stress value);

R, radius of the disc;

R_a, support radius.

The parameter λ accounts for the stiffening effect of an edge overhang of the tested disc over the support.

Eq. (1) predicts obviously infinite tensile stresses in the centre of the disc when the contact radius b approaches zero: $\lim_{b \to 0} \sigma_{max} = -\infty$. Therefore, this theory cannot be used to calculate stresses underneath the loading point.

Kirstein and Woolley, and later Vitman and Pukh[12] extended this solution to a disc loaded with a constant pressure within the centred circular area with radius b. Their solution for the stress field (i.e. the radial and tangential stress components σ_{rr} and $\sigma_{\varphi\varphi}$, defined in a polar coordinate system) on the tensile surface of the disc is claimed to be applicable outside the loading area ($r > b$):

$$\sigma_{rr}(r) = \frac{3 \cdot F \cdot (1 + \nu)}{4 \cdot \pi \cdot t^2}$$
$$\times \left[2 \cdot \ln \frac{R_a}{r} + \frac{(1 - \nu)}{2(1 + \nu)} \cdot \left(\frac{R_a^2 - r^2}{R_a^2} \right) \cdot \frac{b^2}{r^2} \cdot \frac{R_a^2}{R^2} \right], \quad (4)$$

$$\sigma_{\varphi\varphi}(r) = \frac{3 \cdot F \cdot (1 + \nu)}{4 \cdot \pi \cdot t^2}$$
$$\times \left[2 \cdot \ln \frac{R_a}{r} + \frac{(1 - \nu)}{2(1 + \nu)} \cdot \left(4 - \frac{b^2}{r^2} \right) \cdot \frac{R_a^2}{R^2} \right]. \quad (5)$$

The variable r is the distance from the centre at the tensile loaded disc face (i.e. the radius in a polar coordinate system). The stress distribution for $r > b$ depends strongly on the loading area radius b and the problem of diverging stresses for "point-like" forces still remains.

To apply this solution to a ball loaded disc the contact radius b has to be known. Various approximations have been offered to determine this parameter. With the following abbreviations

$$\zeta = \left(\frac{3 \cdot F \cdot R_b}{4 \cdot E'} \right)^{1/3} \quad (6)$$

and

$$\frac{1}{E'} = \frac{(1 - \nu_b^2)}{E_b} + \frac{(1 - \nu^2)}{E}, \quad (7)$$

and with

R_b,   Radius of ball;
ν_b,   Poisson's ratio for ball material;
E_b,   Young's modulus for ball material;
E,   Young's modulus for disc material;

the most common approximations for the contact radius b, found in literature, are listed in Table 2.

These solutions have to be extended for the tensile loaded area underneath the loading area. For the ball on ring of balls geometry Shetty et al.[15] developed an equation to approximate the maximum tensile stress component in the disc (that is at the point $r = 0$ on the tensile stressed surface of the disc) starting from quite similar assumptions as Kirstein and Woolley[8] and Vitman and Pukh:[12]

$$\sigma_{max} = \frac{3 \cdot F \cdot (1 + \nu)}{4 \cdot \pi \cdot t^2}$$
$$\times \left[1 + 2 \cdot \ln \frac{R_a}{b} + \frac{(1 - \nu)}{(1 + \nu)} \cdot \left(1 - \frac{b^2}{2 \cdot R_a^2} \right) \cdot \frac{R_a^2}{R^2} \right]. \quad (8)$$

Kirstein and Woolley[8] claimed that this solution should approximately be independent from the number of supporting balls, so it can be applied to axi- but also to non-strictly axi-symmetric testing configurations.

Another approximation is given by Timoshenko.[16] He modelled a plate without any overhang (i.e. $R = R_a$) and derives a solution for the maximum tensile stress in the disc, which, in addition to other parameters, depends on the ratio of the contact radius to disc thickness: b/t. He assumed that for very small contact radii, the maximum tensile stress is independent on the ratio b/t, getting:

$$\sigma_{max} = \frac{F}{t^2} \cdot \left\{ (1 + \nu) \left[0.485 \ln \left(\frac{R_a}{t} \right) + 0.52 \right] + 0.48 \right\}. \quad (9)$$

The constant numbers were obtained by fitting results of finite-element calculations. All these approximations give quite different solutions for the maximum tensile stress component and the tensile stress distribution in ball on three balls loaded discs. It is obvious that a precise analytical approximation is hard to determine, since this problem has to be solved in three dimensions. Therefore a finite element analysis has been performed to determine the tensile stress field in the loaded disc and the results are presented in the next chapter.

3. Numerical determination of the stress field

In a first approach a (non-linear) contact mechanical analysis was performed by using the commercial finite element (FE) software ANSYS, Version 5.6. The disc and the supporting balls were modelled using brick elements (8 or 20 nodes per element) and the contacts between the balls and the disc were modelled by surface-to-surface contact elements. It is assumed that friction effects only slightly change the stress distribution and is therefore not taken into account in this paper but will be investigated in the following publication. Due to the

mirror symmetry of the system only one sixth of the testing geometry is modelled (Fig. 1). In order to describe the behaviour of the balls in the test assembly,
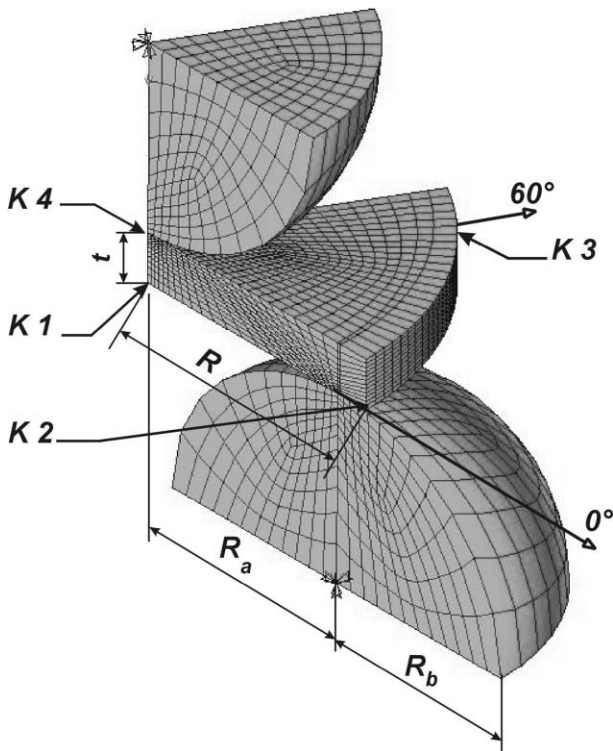

Fig. 1. FE-model of the ball on three balls test assembly: the midpoint of the support ball is fixed and the midpoint of the centred loading ball is only allowed to move vertically; the radii of the supporting balls and of the loading ball are chosen to be equal. Assuming contact between the support balls the relation $R_a = 2\sqrt{3}R_b/3$ holds. Nodes in the symmetry planes (i.e. 0 and 60°) are fixed to them. Special points of interest (so-called key-points K1 to K4) for the following analysis are indicated by arrows.

- the centre of the support balls (lower balls) are fixed in their position,
- their radii are defined to be equal to that of the loading ball and
- they are assumed to be made of the same material,
- the centre of the loading ball (upper ball) is allowed to move only perpendicular to the disc surface (y-direction) to apply the load on the disc,
- in the test assembly described, the support radius R_a is given by the radius of the support balls R_b in that way that the three support balls touch each other, forming an equally sided triangle of support points:

$$R_a = \frac{2\sqrt{3}}{3} R_b. \tag{10}$$

Since most ceramics are well described as isotropic, brittle materials, the materials are modelled as isotropic, homogeneous and linear-elastic continua defined by Young's modulus E and Poisson's ratio ν.

In Fig. 2a and b an example stress distribution is shown. The geometric and materials parameters listed in the description of the Fig. 2a and b define the standard model for this article, referred to in the following chapters if any differing parameter values are not mentioned. These colorcoded overview pictures of the first principal stress distribution (i.e. the largest stress component) show some main features of this test:

- the maximum tensile stress occurs in the centre of the tensile surface of the disc (red area),
- the stress field shows a threefold symmetry, caused by the three supporting balls and
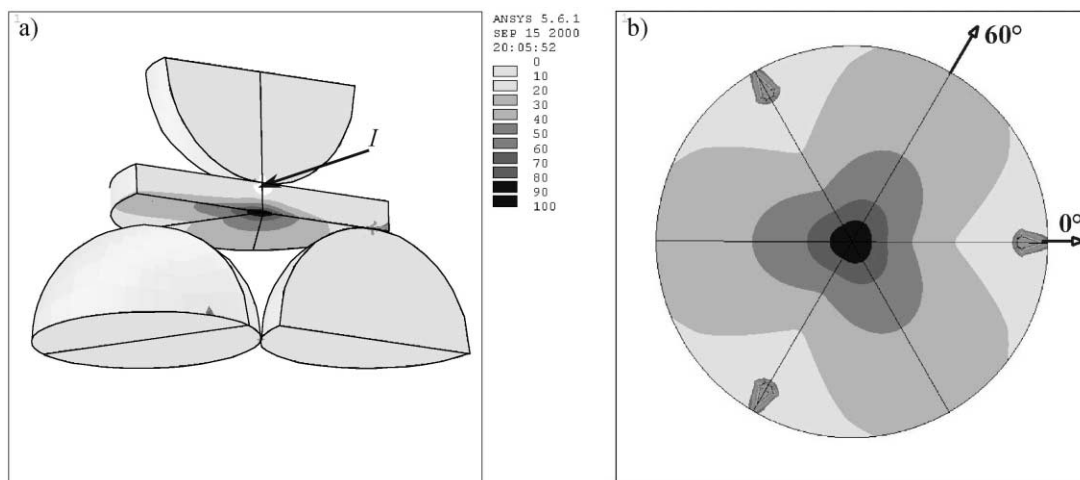- at the support areas compressive stresses occur (grey shaded areas).

Fig. 2. Example of a stress field in a disc for a typical loading condition in a ball on three balls-test, half model. Plotted is the percentage of the maximum tensile stress component in the disc (0–100%). Chosen parameters for the standard model are: $t = 2$ mm, $R = 10$ mm ($t/R = 0.2$), $R_b = 7.535$ mm ($R_a/R = 0.87$), $E = 100$ GPa, $\nu = 0.3$, $E_b = 100$ GPa, and $\nu_b = 0.3$. (a) Positive (tensile) first principal stresses; diagonal view of the disc and the loading and support balls. (b) Positive (tensile) first principal stresses, bottom view of the tensile stress surface of the disc. The white areas, indicated with an arrow (I), stand for compressive stresses, as they arise in the contact area between support balls and the disc.

More detailed information about the tensorial stress field is shown Fig. 3a–c, where results of stress components are plotted along selected paths in the planes of symmetry. The stresses are normalised with the maximum tensile stress value in the centre σ_{max} and the space coordinates with the path lengths. Along the 0°-direction of the tensile surface between Point K1 and K2 (Fig. 3a) the tangential stress components $\sigma_{\varphi\varphi}$ are almost equal to the radial components σ_{rr} in a large range along the radius of the disc and tend to an axisymmetric biaxial stress state at the midpoint. The axial stress σ_{zz} components are zero in this region, since the surface is free. In the contact area (at $r/R = 0.87$)
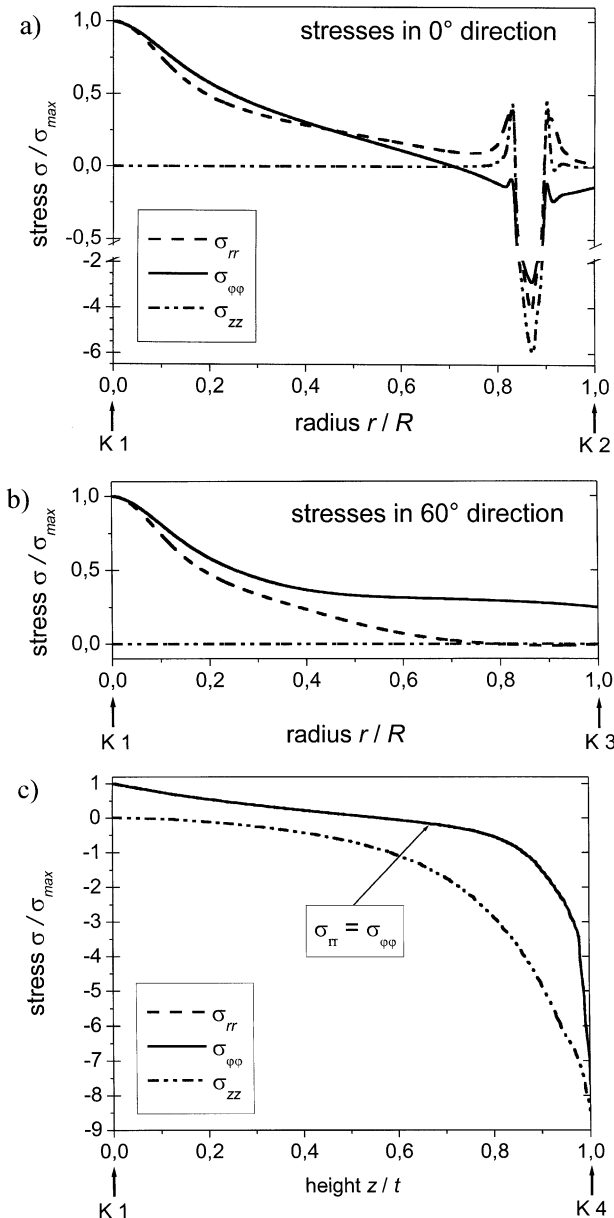

Fig. 3. Radial, tangential and axial normalised stress components. (a) Along a path in the 0°-direction (K1–K2), (b) along the 60°-direction of the tensile plane of the disc (K1–K3) and (c) along the axis of the disc (K1–K4).

between the support ball and the disc, compressive stresses with comparable large magnitudes occur. As known from the Hertzian contact problem[1] also tangential and radial tensile stresses exist around the contact area. For supporting balls with small radii these stresses could even be higher than the stresses in the centre of the disc's surface. Then fracture of the disc is expected to start from the support area. Failure modes of this kind should be avoided since they cannot be interpreted within the scope and the results of this paper. In the 60°-direction of the tensile surface between point K1 and K3 (Fig. 3b) the tangential stress components are higher than the radial stress components, except at the centre where these stress components are approaching each other again. The axial stress components are zero along the whole path. In Fig. 3c the stress components along the vertical axis of the disc between K1 and K4 are shown. At this central path of symmetry the radial and tangential stress components are equal and build up an axis symmetric stress state. It can be recognised, that the absolute value of the compressive stress amplitudes underneath the upper loading ball is several times higher than the amplitude of the tensile stresses in the centre of the tensile surface. The magnitude of the compressive stress maximum can be reduced by enlarging the loading ball. The compressive stress maxima at the supporting balls on the opposite disc plane are significantly smaller (using four identical balls for loading and support), since there are three balls splitting up the total load. But in general the occurrence of comparable large compressive stresses makes this type of test only valuable for materials with a much higher compressive then tensile strength as it holds for ceramic materials.

With this model a parametric study was carried out in order to verify the quality of the analytical solutions. As in all cases of bent plates (or beams) the maximum tensile stress in the disc σ_{max} scales with the applied force F, and with the inverse square of the thickness of the plate t:

$$\sigma_{max} = f \cdot \frac{F}{t^2}. \tag{11}$$

Therefore, the factor f is dimensionless. In this equation also the effect of the Hertzian flattening of the balls is taken into account. According to isotropic linear-elastic material properties and the involved geometry factors the stress field in the disc depends on eight parameters (geometrical, material and loading parameters). In general these eight parameters are arguments of the function f:

---

[1] The formulation and solution of the Hertzian contact problem can be found in many standard book of mechanics; for example.[17]

- the force F,
- the support radius R_a [see Eq. (10)], the disc radius R, and the disc thickness t,
- the elastic constants of the disc E and ν (Young's modulus and Poisson's ratio) and
- the corresponding elastic constants of the balls (load, support) material E_b and ν_b.

With the investigated testing method it is intended to measure the strength of brittle and hard materials. This task limits the range of relevant material parameters to stiff metallic and ceramic materials. In the present investigation

- the Young's moduli E and E_b are varied from 100 to 1000 GPa and
- the Poisson's ratios ν and ν_b are varied from 0.2 to 0.3.

3.1. Influence of the contact radius on the tensile stresses in the disc

During the loading the central ball and the disc deform so that a circular contact area of radius b builds up under the loading ball (a smaller contact area builds up over each of the three supporting balls). With increasing load the contact area increases. Of course this contact area depends on the applied force and is the greater the softer the support and disc materials are. This change in the loading geometry may also influence the tensile stresses in the disc. Following the analytical approximations for the maximum tensile stress (discussed in Section 2) a strong dependency of the tensile stresses on the contact radius can be expected. This relationship is investigated in the following.

For the example described in Fig. 2, ($R = 10$ mm, $t = 2$ mm, $R_b = 7.535$ mm, $\nu = \nu_b = 0.3$) the contact radius b is plotted versus the applied force in Fig. 4. Different symbols refer to different combinations of the Young's moduli of the ball and disc materials (E, E_b). Generally for a given combination of material properties the contact radius increases nonlinearly with the applied force. But the contact radius is also a function of the elastic moduli: the deformation is larger for a combination of low modulus ball and disc materials (case of $E = E_b = 100$ GPa, square symbols) and it is smaller for a combination of high modulus materials (case of $E = E_b = 400$ GPa, circle symbols). It is interesting to note, that it does almost not depend whether the disc or the ball material is stiffer: the symbols for the case $E = 100$ GPa and $E_b = 400$ GPa (cross symbols) coincides with the inverse case of a combination $E = 400$ GPa and $E_b = 100$ GPa (star symbols).

The lines in Fig. 4 refer to the analytical expressions listed in Table 2. The approximation of Godfrey,[10] evaluated at $E = E_b = 100$ GPa (solid line) almost coincides
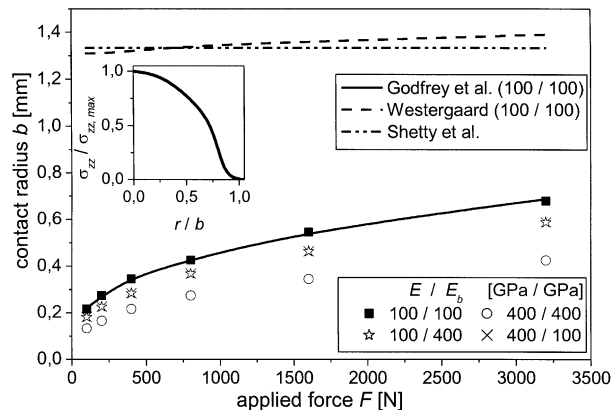

Fig. 4. Contact radius b, as a function of the applied load F for different combinations of Young's moduli of ball and disc. The other parameters are the same as used in Fig. 2 (b was gained from the calculated radius where the contact force on the disc applied by the ball dropped to zero). Also shown are the results of some analytical approximations for $E = E_b = 100$ GPa.

with the numerical solutions. Actually all drawn data points for various combinations of Young's moduli can be reproduced by the formula of Godfrey within a few percents of deviation. The solutions of Westergaard[14] (dashed line) or Shetty et al.[15] (dotted line) drastically overestimate the contact radius.

Additional calculations for support materials with other Poisson's ratios (ν_b was varied from 0.2 to 0.3) result in such small differences to the plotted results (less than 1%), that they can not be recognised in the diagram. If the load transfer from the support in the disc is not influenced by the change of ν_b, the stress field in the disc can it be neither. Therefore, the influence of ν_b, on the stress field in the disc is neglected in the further investigations.

The insert in Fig. 4 presents FEM-calculation results of the contact pressure distribution (under the loading ball, i.e. in the top plane of the disc) in an invariant way. By drawing the pressure in units of the maximum contact pressure and the radius in units of the contact radius b, a parabolic-type pressure distribution is obtained, which is nearly the same for all relevant test situations. This result shows clearly that the pressure is distributed and not constant as assumed in the analytical approximations discussed in Section 2.

Fig. 5 shows the dependency of the dimensionless factor f [the highest tensile stress component σ_{max} in the disc, divided by the scaling stress F/t^2, compare Eq. (11)] versus the applied force, F. The square symbol represents the FEM-results for the standard model (compare Fig. 2), while the four other symbols correspond to modified models. It can clearly be seen, that—in the parameter range investigated—this factor f does not depend on the applied force, it is constant for one set of parameters. This result is not trivial since the contact areas between ball and disc increase non-linearly with
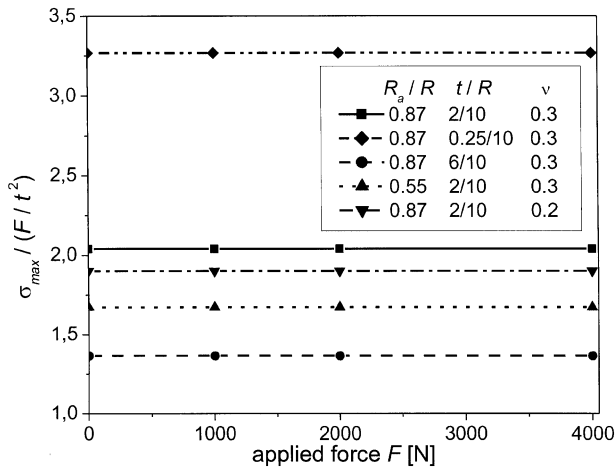
Fig. 5. Maximum tensile stress component (at $r = 0$) normalized with F/t^2 versus the applied load. Data for several different combinations of ball and disc materials (E and E_b) are shown. The other used parameters are equal to the parameters used in Fig. 2.

Fig. 6. Tensile stress distribution in the bottom plane of the disc along the 0°- and the 60°-directions for two values of Young's modulus of the disc's material in dimensionless variables. The other parameters are equal to those in Fig. 2. The stress results for the case for $E = 100$ GPa, as shown in Fig. 3a and b in detail, is also shown for a point loading, which is drawn as solid (0°) and dashed line (60°). The corresponding results coincide in the considered range within a deviation less than 1%.

increasing force. Another source of force-dependence and non-linearity, namely the geometric non-linearity, is negligible, since the strains in stiff materials are "small" under the considered loading situations.

Finally the dependence of the tensile stress field is examined for various combinations of Young's moduli. A normalized plot of the 1st principal stresses along the path in 0 and 60° direction is shown in Fig. 6 for two different Young's moduli of the disc (symbols) as an example. Actually all combinations of elastic constants within the given parameter range lead to the same tensile stress field opposite to the loading ball within a deviation smaller than 1% (excepted is the direct contact area between support balls and disc). Therefore, the factor f in Eq. (11) can be assumed to be independent from the applied force, the elastic moduli of the balls material (i.e. E_b, v_b) and the Young's modulus of the disc material E. This reduces the number of independent variables influencing the tensile stress field in the disc to three (the ratio R_a/R, the ratio t/R and the Poisson's ratio of the disc v).

Also included in Fig. 6 are results of calculations made for a point-loaded disc. These results coincide with the results for the ball-loaded discs. The calculations were made for typical testing geometries ($t/R > 0.05$). In this parameter range the loaded area is far enough from the tensile side of the disc that it makes no difference for the tensile stresses whether the loading force is applied in a very small (point-like) or a larger loading area. This observation leads to a further important simplification of the FE-model: to describe the tensile stress field properly, it is sufficient to model the loading with point loads: the complicated non-linear modelling of the loading area with contact elements is not necessary. Therefore, the following calculations are made with the simpler point-loading model. It should be
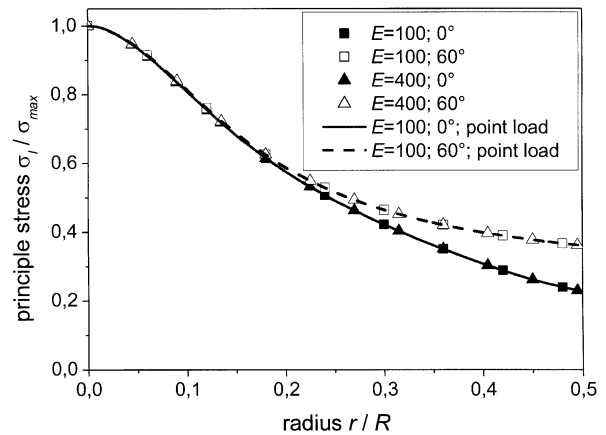
mentioned that this is in conflict with the analytical approximations reported in Section 2, where the contact radius has a significant influence on the tensile stress field. In fact the contact radius has been used to calibrate the results: The approximation of Shetty et al.[15] for the stress field has a fair coincidence with the FE-results of this work but the contact radius is overestimated for several times (see Fig. 4). In the case of the approximation of Godfrey[10] and Godfrey and John[6] the contact radius fairly corresponds to our FE-results but the tensile stress field does not.

It should be noticed that these results are not restricted to the standard model described in Fig. 3. They are valid for a wide range of disc and support geometries. It can be expected that the approximations will fail for too thin and too thick discs. Therefore the validity of the assumptions were checked for disc thickness to disc radius ratios in the range of $0.05 < t/R < 0.6$, which seems to be appropriate for most cases of practical relevance. The overhang of the disc over the support has no influence on the validity of the suggested approximations.

3.2. The maximum tensile stress amplitude in the disc

In the centre of the bottom (tensile) plane of the disc exists a biaxial stress state, the amplitudes of the radial and tangential stress components are described by the factor f [Eq. (11)]. Following the ideas of the last chapter, there are only three remaining parameters, which influence this factor: the geometric parameters t/R and R_a/R and the Poisson's ratio of the disc material, v. A large number of FE calculations were done to achieve a field of parameters that cover most of the most common

testing geometries and Poisson's ratios. The investigated range of parameters is listed in Table 3. The dependence of the factor f on these three parameters is shown in Fig. 7.

It can be recognised, that an overhang of the disc over the support stiffens the specimen and reduces the maximum tensile stress. For the same reason the maximum tensile stresses are higher for thin slices than for thick discs.

To be able to evaluate tests using the factor f, an analytical equation is useful. A non-linear fit of the calculated data points according to expression (12) was performed using MATHEMATICA Version 4.1. The seven constants c_i ($i = 0,\ldots6$) were calculated for three specific Poisson's ratios 0.2, 0.25 and 0.3 and are listed in Table 4.

$$f\left(\frac{t}{R}, \frac{R_a}{R}, \nu\right) = c_0$$
$$+ \frac{\left(c_1 + c_2\frac{t}{R} + c_3\left(\frac{t}{R}\right)^2 + c_4\left(\frac{t}{R}\right)^3\right)}{1 + c_5\frac{t}{R}}\left(1 + c_6\frac{R_a}{R}\right) \quad (12)$$

These equations fit the maximum tensile stresses with an error of less than 0.5% for the whole evaluated range of parameters. For Poisson ratios ν between 0.20 and 0.25 or between 0.25 and 0.3, respectively, f can be linearly interpolated between corresponding values $f(\nu_1)$ and $f(\nu_2)$ according to

Table 3
Evaluated range of independent parameters for the factor f

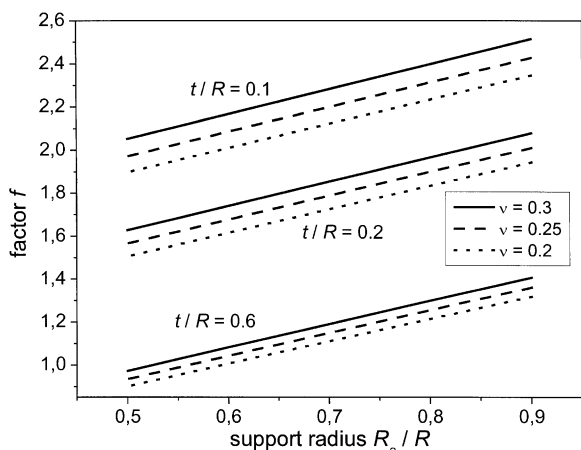| Parameter	Evaluated range
R_a/R	0.55–0.9
t/R	0.05–0.6
ν_d	0.20–0.3

Fig. 7. Factor f (maximum tensile stress amplitude in the disc normalised with the stress F/t^2) versus the ratio of R_a/R. The curves refer to different ratios of thickness to disc radius t/R. Full lines: $\nu_d = 0.3$, dashed lines: $\nu = 0.25$, dotted lines: $\nu = 0.2$.

Table 4
Calculated values for the constants c_i used in Eq. (12) for three different Poisson's ratios

	$\nu = 0.2$	$\nu = 0.25$	$\nu = 0.3$
c_0	−12.354	−14.671	−17.346
c_1	15.549	17.988	20.774
c_2	489.2	567.22	622.62
c_3	−78.707	−80.945	−76.879
c_4	52.216	53.486	50.383
c_5	36.554	36.01	33.736
c_6	0.082	0.0709	0.0613

$$f\left(\frac{t}{R}, \frac{R_a}{R}, \nu\right) = \frac{\nu_2 - \nu}{\nu_2 - \nu_1}f\left(\frac{t}{R}, \frac{R_a}{R}, \nu_1\right)$$
$$+ \frac{\nu - \nu_1}{\nu_2 - \nu_1}f\left(\frac{t}{R}, \frac{R_a}{R}, \nu_2\right) \quad (13)$$

Using this result the maximum tensile stress in the disc can be calculated for the most common disc and support geometries.

A comparison of the analytical solutions discussed in Section 2 with the results of the FE-calculations of this work shows, that the approximations of Shetty et al.[15] and Westergaard[14] describe the maximum tensile stress component in the disc fairly well. For not too thin discs ($t/R > 0.05$) their results deviate from the FE-solutions less than 2%, but for thinner discs the deviations may be much higher. The other approximations are less precise. In the case of the approximation of Godfrey[10] and Godfrey and John[6] the deviations from the FE-solutions can exceed 100%.

The model can fail for two reasons:

1. if the specimen is too thick or the radius of the loading ball is to small the fracture could be induced by Hertzian contact stresses and
2. if the specimen is too thin and its elastic modulus is too low buckling may occur.

Both failure modes are not likely to occur in the range of parameters investigated (Table 3).

4. Experimental investigations

To gain some experimental evidence on the applicability of the ball on three balls test fracture experiments were performed. The locations of the fracture origin were recorded to proof whether the fracture origin occurs in the theoretical predicted area of maximum stress (i.e. in the centre of the tensile loaded surface of the disc). Strength data of discs were compared with those on bent beams.

The fracture tests were performed on a commercial alumina quality (AL23 by Friatec GmbH, BRD). The material was provided as uniaxially pressed discs. Their diameter varied from 20.20 to 20.24 mm and their

thickness from 2.96 to 3.00 mm. For the values of the elastic constants the manufacturer's data sheet states $E = 380$ GPa and $\nu = 0.22$ respectively.

The tests were performed on "as sintered" and on "machined" discs. In the latter case, the finishing steps followed the suggestions given in DIN 51 110[18] (i.e. a grinding finish with diamond grit D15 on the prospective tensile surface). The bending bars were machined from the supplied discs to a size of $15 \times 2 \times 1.5$ mm^3. Again specimens with an "as sintered" and a finished surface according to DIN 51 110 were produced.

For the ball on three balls-tests a special fixture has been designed. Special care was taken, that the specimen, the supporting and the loading balls can be exactly centred. Bearing balls made from a hardened steel were used for the supporting balls. Their elastic constants are $E_b = 210$ GPa and $\nu_b = 0.3$. The diameter of the balls is $R_b = 7.535$ mm. The fixture in the experimental procedure are described in more detail in.[19] For the reported tests the ratio describing the overhang of the discs over the support is $R_a/R \cong 0.87$ and the ratio describing the shape of the discs is $t/R \cong 0.3$. A crosshead speed of 1 mm/min lead to fracture after 10–15 s.

The bars were broken using fixtures with an outer support span of 13 mm and an inner support span of 4.33 mm on a Zwick universal testing machine.[20] A crosshead speed of 0.75 mm/min was applied to achieve failure within 10–15 s.

In all fractured discs, the fracture initiated in the tensile surface plane underneath the loading ball. Failure with

Fig. 8. Fracture patterns of Al$_2$O$_3$ discs tested in the ball on three balls test assembly. The circles show the area of the fracture origin.

a threefold symmetry dominates, but in a few cases the disc breaks into two or four pieces (Fig. 8). Tentatively it was found the number of fracture pieces increases with strength (stored elastic energy). In all investigated cases the fracture origin was at or very near to the tensile surface (Fig. 9a and b) and looked similar in disc as well as in bending specimen. A magnification of the fracture origin showed no significant defects which indicates that weak boundaries (in the case of as sintered surfaces) or machining defects (in the case of grinded surfaces) were the initiations sites for fracture. In no case the fracture started from the area around the loading ball, were also tensile stresses occur. These observations give a clear evidence that the concept of the ball on three balls loading geometry is appropriate.

Following the procedure described in ENV 843-5[22] the characteristic strength σ_0 and the Weibull modulus m as well as the limits of their 95%-confidence intervals (according to[21]) were determined for each set of data. Variations in specimen geometry were taken into account for the evaluation of the fracture stress. Any sample consisted of 30 specimens. These results are listed in Table 5. A first glance at the data shows that the surface finish has some influence on the strength. This fact fits to the observation that always fracture originates at or very near the surface. The Weibull modulus, which describes the relative frequency of flaws sizes, is (almost) equal for samples containing specimens with the same kind of surface finish, but it is different for samples containing specimens of different surface finish.

To compare the characteristic strength values of different sets of data probabilistic fracture mechanics has to be applied. Two effects have influence on the characteristic strength: Multi axial stress states are more searching for defects then uniaxial stress states and large specimens are more prone to contain dangerous defects than small specimens. The first effect is accounted by a fracture criterion for multi axial loading and the second effect is taken into account by the Weibull extrapolation of strength, which predicts lower strength values for larger specimens. Two variants of the Weibull theory
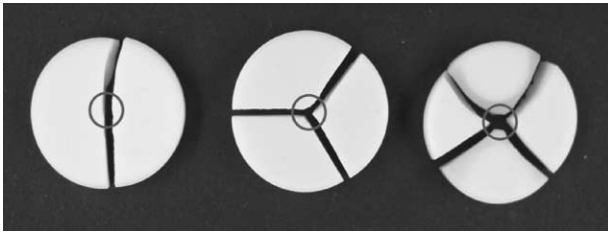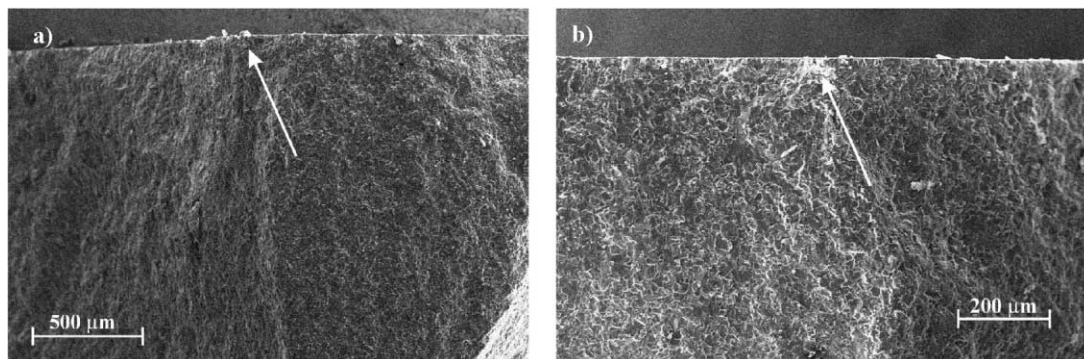

Fig. 9. (a) and (b) Typical fracture origins on the ball on three balls tested discs. The fracture origin is indicated but no flaws in the microstructure can be identified.

Table 5
Results of the strength measurements with 4-point bending and ball on three balls test[a]

	Test method	σ_0 (MPa)	m	$\sigma_{0,eq}$ (MPa)	$\sigma_{0,eq,V}$ (MPa)	$\sigma_{0,eq,S}$ (MPa)
"As sintered" surface	4-Point bending test	338	15	338	338	338
		330/346	11/18	330/346	330/346	330/346
	Ball on three balls test	348	17	363	357	334
		343/354	14/21	358/370	352/363	329/340
Ground surface	4-Point bending test	365	21.0	365	365	365
		359/371	16/26	359/371	359/371	359/371
	Ball on three balls test	385	21	398	386	371
		380/390	16/26	393/403	381/391	366/376

[a] Listed are the values for σ_0 and m and the limits of the corresponding 95% confidence interval. Also listed are the equivalent stress, $\sigma_{0,eq}$, which accounts for the multiaxiality of the stress state and the Weibull extrapolated strength values, $\sigma_{0,eq,V}$ and $\sigma_{0,eq,S}$, which respectively account for the different volume and surface of the disc specimens and bending specimens.

are often used accounting for volume and the surface flaws respectively. The relevant information on the proper definition of the equivalent stress and on the size effect can be found in standard textbooks on probabilistic fracture mechanics.[23,24] More information on the influence of multi axial stresses can be found in[25,26,28,29] and on the size effect of strength in.[21,30,31]

In the following the characteristic strength data gained on discs are used to predict the characteristic strength of the beams. To account for the multi axial loading an equivalent stress, σ_{eq}, an often used multiaxial failure criterion—the principle of independent action[25,26,27]—is applied. This stress corresponds to the fracture stress in an uniaxialy loaded specimen of same (effective) size. For more details see.[25] Then the Weibull theory is used to extrapolate this stress from specimens of the (effective) size of the discs to that of the beams. This can be done for specimens containing volume or surface flaws giving the strength values $\sigma_{eq,V}$ and $\sigma_{eq,S}$ respectively. For the calculation, the ratio of the effective volumes[22] (or the effective surfaces) of the discs and the beams has to be known. This ratio has been calculated to be 0.75 for the specimens with the "as sintered" surface and to be 0.52 for the specimens with the ground surface (the ratio of effective surfaces is 0.19 and 0.13 for both surface conditions respectively). The data extrapolation and the calculation of effective volume and surface will be described in more details in a subsequent paper.[19] The calculated stresses are also plotted in Table 5.

Using the volume flaw model the predicted characteristic strength is 357 MPa for the as sintered surface state. The measured value is 338 MPa. In the case of the grinded specimens, the values are 386 and 365 MPa respectively. The strength of the bending bars is predicted with a scatter of less than 5%, which seems to be fair, if possible experimental errors[19] are taken into account. Using the surface flaw model the extrapolated strength is 334 MPa compared to the measured value of 338 MPa for the specimens with an as sintered surface and 371 MPa compared to 365 MPa for the specimens with the grinded surface. In this case, the 95% confidence intervals

overlap indicating that the underlying models are correct. This fact is also supported by fractographic evidence.

To summarise no experimental evidence could be found that the proposed fracture test and the theoretical evaluation of the data are not appropriate.

5. Summary and concluding remarks

The ball on three balls testing geometry for biaxial strength testing of brittle materials has some advantages compared to other testing assemblies, especially it is not sensitive for an out of flatness of the specimen. This fact makes it possible to test ceramic discs in the as sintered surface state. The most important disadvantage of the ball on three balls testing geometry is, that the stress state has a threefold symmetry and that it may depend on a large number of geometrical and material parameters making analytical approximation difficult. The FE-analysis performed in this paper shows, that—in the parameter range investigated (which covers the most important combinations of parameters for strength testing of discs made from hard and brittle materials)—some very important simplifications are possible. It could be shown, that the stress field in the disc;

- does not depend on the elastic constants of the supporting balls and the loading ball,
- it does not depend on the Young's modulus of the tested material (but it depends on its Poisson's ratio) and
- the amplitude of the stress field scales with the applied load.

These results suggest, that—in the parameter range investigated—the stress field in the disc does not depend on the nonlinear changes in the loading geometry, which are primarily caused by the deformation of the balls. Indeed, it could also be shown, that the loading situation (ball loading) can be approximated by a simple point loading mode with a high degree of accuracy.

This approximation makes the necessary FE-model much simpler and the numerical calculations much faster.

The maximum tensile stress component, σ_{max}, occurs in the centre of the surface plane of the disc underneath the loading ball, where the stress state is purely biaxial. In the region around this maximum (which is significant for the strength of the disc) the stress state scales with the maximum tensile stress component.

Tensile stresses (Hertzian stresses) also occur around the loading areas caused by the loading and supporting balls. They will be higher the smaller the radius of the balls. This may limit the minimum size of the balls. Fractography has to be used to identify whether fracture is initiated by the accounted stresses in the centre of the disc surface and not by the Herzian stresses around the loading ball. In the 60 fracture experiments performed on a commercial aluminia ceramic, fracture always started at the expected area.

The maximum tensile stress component, σ_{max}, is

- proportional to the applied force, F, and it is
- indirectly proportional to the square of the disc thickness, t: $\sigma_{max} = f \cdot \frac{F}{t^2}$.

The factor f still depends on the loading geometry, the specimen geometry and the Poisson's ratio of the tested material. The first situation is expressed by the ratio of the support radius to the radius of the disc and the second by the ratio of the disc thickness to the disc radius. An analytical expression for the factor f is presented, which has been fitted to the numerical results and which describe them with an error of less than 1%.

Fracture experiments on discs and on bars were performed on specimen made of an alumina ceramic with two different surface states. A comparison of the results of ball on three balls tests and bending tests needs the conversion of strength data using probabilistic fracture mechanics. Within the natural scatter of the strength of the investigated material the strength of the different sets of specimens was equal. This is an experimental indication, that the investigated method is fairly well situated to describe the tensile strength of brittle materials.

In a consecutive paper[19] details on a possible experimental set up will be discussed. The possible experimental scatter of this set up will also be discussed in detail. The method of converting biaxial to uniaxial data including the choice of a suitable multiaxial fracture criterion and of a suitable size extrapolation of data will also be tackled. In this context the effective volume and the effective surface of the ball on tree balls tested discs according to the Weibull theory will be calculated.

References

1. de With, G. and Wagemans, H. M., Ball-on-ring test revisited. *J. Am. Ceram. Soc.*, 1989, **72**, 1538–1541.

2. Morrell, R., McCormick, N. J., Bevan, J., Lodeiro, M. and Margetson, J., Biaxial disc flexure-modulus and strength testing. *Bri. Ceram. Trans.*, 1999, **98**, 234–240.

3. Soltesz, U., Richter, H. and Kiezler, R., *Proceedings of Conference Ceramics in Clinical Applications*. Elsevier, Milan, 1986.

4. Fessler, H. and Fricker, D. C., A theoretical analysis of the ring-on-ring loading disk test. *J. Am. Ceram. Soc.*, 1984, **67**, 582–588 (correction: 1988, **71**(10), 904).

5. Matthewson, M. J. and Field, J. E., *J. Phys. Eng. Sci. Instrum.*, 1980, **13**(3), 355–359.

6. Godfrey, D. J. and John, S., Disc flexure tests for the evaluation of ceramic strength, In *Proceedings 2nd International Conference of Ceramic materials and Components for Engines*. Verlag Deutsche Keramische Gesellschaft, Lübeck-Travemünde, 14–17 April 1986, pp. 657–665.

7. ASTM F 394-78 (reapproved 1996), Standard test method for biaxial flexure test (modulus of rupture) of ceramic substrates.

8. Kirstein, A. F. and Woolley, R. M., Symmetrical bending of thin circular elastic plates on equally spaced point supports. *J. Res. Natl. Bur. Stand., Sect. C*, 1967, **71**, 1–10.

9. Byrne, W. P. and Morrell, R., *Results of the UK Interlaboratory Strength Test Exercise. NPL Report CMMT (A) 296*, November 2000.

10. Godfrey, D. J., Fabrication, formulation, mechanical properties, and oxidation of sintered Si3N4 ceramics using disc specimens. *Mater. Sci. Technol.*, 1985, **1**, 510–515.

11. Bassali, W. A., The transverse flexure of thin elastic plates supported at several points. *Proceedings of the Cambridge Philosophic Society*, 1957, **53**, 728–743.

12. Vitman, F. F. and Pukh, V. P., A method for determining the strength of sheet glass. *Zavod. Lab.*, 1963, **29**, 863–867.

13. Standard ISO 6474, *Implants for Surgery—Ceramic Materials Based on High Purity Alumina*, 1994.

14. Westergaard, H. M., Stresses in concrete pavements computed by theoretical analysis. *Public Roads*, 1926, **7**, 25–35.

15. Shetty, D. K., Rosenfield, A. R., McGuire, P., Bansal, G. K. and Duckworth, W. H., Biaxial flexure test for ceramics. *Ceramic Bulletin*, 1980, **59**, 1193–1997.

16. Timoshenko, S. P. and Woinowsky-Krieger, S., *Theory of Plates and Shells*, 2nd edn. McGraw-Hill International Editions, New York, 1959.

17. Timoshenko, S. P. and Goodier, J. N., *Theory of Elasticity*, 3rd edn. McGraw-HillBook Company, 1970.

18. DIN EN 843-1, *Prüfung von keramischen Hochleistungswerkstoffen: 4-Punkt-Biegeversuch bei Raumtemperatur*, Standard, 1990.

19. Börger A., Supancic P. and Danzer R., The ball on three balls test—experimental set up, failure analysis and test evaluation (in preparation).

20. Lube, T., Manner, M. and Danzer, R., The miniaturisation of the 4-point bend test. *Fatigue Fract. Eng. Mater. Struct.*, 1997, **20**, 1605–1616.

21. Danzer, R., Lube, T. and Supancic, P., Monte-Carlo simulations of strength distributions of brittle materials—type of distribution, specimen- and sample size. Submitted to: *Zeitschrift für Metallkunde*.

22. DIN ENV 843-5, *Advanced Technical Ceramics: Monolithic Ceramics Mechanical Tests at Room Temperature Part 5: Statistical Analysis*, Standard, 1997.

23. Munz, D. and Fett, T., *Ceramics*. Springer-Verlag, Berlin, 1999.

24. Wachtman, J. B., *Mechanical Properties of Ceramics*. John Wiley & Sons, New York, 1996.

25. Freudenthal, A., A statistical approach to brittle fracture. *Fracture*, 591–619.

26. Barnett, R., Hermann, P., Wingfield, J. and Conners, C., Fracture of brittle material under transient mechanical and thermal loading. *Technical Report AFFDL-TR-66-220*, 1986, Air Force Flight Dynamics Laboratory, Ohio.

27. Krüger, S., *Ein Beitrag zur Praxisgerechten Dimensionierung keramischer Bauteile bei mehrachsigen Beanspruchungen*, Dissertation, TU Clausthal, October 1999.

28. Wei-Sheng, Lei, *Statistics of brittle fracture under multiaxial loading*, Dissertation, Aachen, February 1999.

29. Thiemeier, T., *Lebensdauervorhersage für keramische Bauteile unter mehrachsiger Beanspruchung*, Dissertation, Univ. Karlsruhe, 1989.

30. Weibull, W., A statistical distribution function of wide applicability. *J. Appl. Mech.*, 1951, **18**, 253.

31. Danzer, R., A general strength distribution function for brittle materials. *J. Eur. Ceram. Soc.*, 1992, **10**, 461–472.